Astronomy & Astrophysics manuscript no. 5505ms
June 19, 2006

Star formation in the vicinity of the IC 348 cluster

M. Tafalla[1], M. S. N. Kumar[2], and R. Bachiller[1]

[1] Observatorio Astronómico Nacional (IGN), Alfonso XII 3, E-28014 Madrid, Spain
[2] Centro de Astrofísica da Universidade do Porto, Rua das Estrelas, 4150-762 Porto, Portugal

Received – / Accepted –

ABSTRACT

Aims. We present molecular line observations of the southwestern part of the IC 348 young cluster, and we use them together with NIR and mm continuum data to determine the distribution of dense gas, search for molecular outflows, and analyze the ongoing star formation activity in the region.

Methods. Our molecular line data consists of $C^{18}O$(1–0) and N_2H^+(1–0) maps obtained with the FCRAO telescope at a resolution of about 50″ and CO(2–1) data obtained with the IRAM 30m telescope at a resolution of 11″.

Results. The dense gas southwest of IC 348 is concentrated in two groups of dense cores, each of them with a few solar masses of material and indications of CO depletion at high density. One of the core groups is actively forming stars, while the other seems starless. There is evidence for at least three bipolar molecular outflows in the region, two of them powered by previously identified Class 0 sources while the other is powered by a still not well characterized low-luminosity object. The ongoing star formation activity is producing a small stellar subgroup in the cluster. Using the observed core characteristics and the star formation rate in the cluster, we propose that that similar episodes of stellar birth may have produced the subclustering seen in the halo of IC 348.

Key words. ISM: jets and outflows, ISM: individual objects: IC 348, stars: formation

1. Introduction

IC 348 is one of the most studied young clusters. Its stellar population has been observed at different wavelengths from the IR to the X rays (Lada & Lada 1995; Luhman et al. 1998; Herbig 1998; Najita et al. 2000; Muench et al. 2003; Preibisch & Zinnecker 2004), and its surrounding gas, part of the Perseus molecular cloud, has been mapped with different resolutions in mm-wave lines and continuum (Bachiller & Cernicharo 1986; Hatchell et al. 2005; Enoch et al. 2006; Ridge et al. 2006; Sun et al. 2006; Kirk et al. 2006). The cluster lies at a distance of 320 pc (e.g., Herbig 1998) and consists of more than 300 stars distributed with a core-halo structure over a region 20 arcminutes in diameter (Muench et al. 2003). Superposed to the smooth distribution of stars, there is a population of stellar groups ("subclusters") each containing 5-20 stars within a radius of 0.1-0.2 pc (Lada & Lada 1995). Most stars in IC 348 have formed at a close-to-constant rate over the last 2-3 Myr, although some cluster members may be significantly older (Herbig 1998; Luhman et al. 1998).

Star formation in IC 348 seems to have ceased toward the center but it continues at some level near its southern border, where the cluster meets the molecular cloud. Strom et al. (1974) identified an IR object to the SW of IC 348 (IC348-IRS1 hereafter), and further observations in the visible and IR by Boulard et al. (1995) have resolved it into a bipolar nebula likely due to an embedded star with a disk. Bachiller et al. (1987) identified several dense cores in its vicinity, and McCaughrean et al. (1994) found additional signposts of recent star formation in the form of shock-excited H_2 emission. The most prominent of these H_2 features is the HH211 flow, which originates from source HH211-MM and is associated with a highly collimated molecular outflow mapped in CO and SiO (Gueth & Guilloteau 1999; Chandler & Richer 2001; Palau et al. 2006; Hirano et al. 2006). Another prominent H_2 feature has been recently associated with an outflow by Eislöffel et al. (2003), who found an additional mm source that seems to power it. The NIR and optical observations of Eislöffel et al. (2003) and Walawender et al. (2005, 2006) reveal multiple HH objects in the region and suggest that additional young stellar objects (YSOs) lie embedded in the dense gas.

In this paper we present the results from a survey of the southwest region of IC 348 (IC348-SW hereafter) aimed to study its star formation activity and the relation between the dense gas and the molecular outflows. These data reveal the presence of several aggregates of dense cores, some of them starless, together with at least three molecular outflows (two

Send offprint requests to: M. Tafalla e-mail: m.tafalla@oan.es

newly mapped in CO), and help clarify the kinematics of both the outflow gas and the dense material. Combining our observations with published IR data, we show that the subclusters in the halo of IC 348 first identified by Lada & Lada (1995) could have originated from star formation episodes inside small core aggregates like the one currently active in IC348-SW.

2. Observations

We observed the IC348-SW region in $C^{18}O$(1–0) and N_2H^+(1–0) with the (then) 16-pixel SEQUOIA array receiver on the FCRAO[1] telescope in 2001 April. The observations were done in frequency switching mode using a correlator that provided velocity resolutions of 0.03 km s^{-1} ($C^{18}O$) and 0.06 km s^{-1} (N_2H^+). The pointing was checked and corrected using observations of SiO masers, and the data were converted into the main-beam temperature scale using an efficiency of 0.55. The FWHM of the telescope beam was approximately 50″.

We observed the vicinity of IC348-IRS1 in the 1.2mm continuum with the MAMBO1 bolometer array at the IRAM 30m telescope in 1999 December. One on-the-fly map was made with a scanning speed of 4″ s^{-1}, a wobbler period of 0.1 s, and a throw of 41″. The atmospheric optical depth was estimated from sky dips carried out immediately before and after the map, and the data were reduced with the NIC software package. We also observed the IC348-SW region simultaneously in CO(1–0) and CO(2–1) with the IRAM 30m telescope in 2000 October and 2001 October. The observations were done in dual-polarization, position switching mode and were centered at α_{2000}=03:43:58.8, δ_{2000}=32:01:51. The reference position was 20 arcminutes north from the map center, and it was checked to be free from detectable emission in the velocity range of interest. A correlator split into four sections provided velocity resolutions of 0.20 and 0.41 km s^{-1} for the 1–0 and 2–1 spectra, respectively. The atmosphere was calibrated by observing ambient and cold loads, and standard efficiency values were used to convert the telescope intensities into the main-beam brightness scale. The pointing was checked making cross scans on bright continuum sources, and the FWHM of the telescope beam was 21″ at the CO(1–0) frequency and 11″ at the CO(2–1) and 1.2mm continuum frequencies.

Near-infrared observations were made using the 3.8m UKIRT with the UIST array camera on the night of 2002 December 5 under excellent seeing conditions (0.5″ in K band). The camera provided a plate scale of 0.12″ per pixel with a total field of view of 120″×120.″ We obtained a 9 point jitter of 60 second exposure time in the K band. Standard procedures for data acquisition and reduction were followed, involving flat fielding, sky, and dark subtraction of the raw frames. The limiting magnitude of the image was 17.6.

3. Large-scale distribution and dense cores

Figure 1 shows in contours our large-scale FCRAO maps of the $C^{18}O$(1–0) (left) and N_2H^+(1–0) (right) emission toward the south-west vicinity of the IC 348 cluster superposed on the 2MASS K-band and Spitzer IRAC1 (3.6 μm) images (see Jørgensen et al. 2006 for full IRAC maps of Perseus). As the $C^{18}O$ map shows, most of the molecular material lies along an arc whose center approximately coincides with the center of the IC 348 cluster and has a radius of about 12′ or 1 pc (see Hatchell et al. 2005 for a complete $C^{18}O$(1–0) map of the region). The dense gas, traced by N_2H^+(1–0) in the right panel, consists of two groups of cores along the $C^{18}O$ arc plus a weaker core to the north, close to the IC 348 center. The western group of cores, which we will refer to as IC348-SW1, was mapped previously in NH_3 by Bachiller et al. (1987). It has an approximate horseshoe shape and consists of three cores named A, B, and C by Bachiller et al. (1987) (see Fig. 1). Some of these cores contain well known young stellar objects (YSOs): core B is associated with IC348-IRS1 (Strom et al. 1974), core C contains HH211-MM (McCaughrean et al. 1994; Gueth & Guilloteau 1999), and between cores B and C lies the mm source IC348 MMS of (Eislöffel et al. 2003). The second group of cores is located to the southeast of IC348-SW1 and will be referred to as IC348-SW2. It consists of two cores, none of them associated with a known YSO or an IRAS source. As Fig. 1 shows, both IC348-SW1 and SW2, and their surrounding molecular gas, coincide with an almost total absence of scattered light at 3.6 μm. This suggests that the two regions lie in the front part of the IC 348 cluster.

The N_2H^+ emission of IC348-SW1 in Fig. 1 is remarkably similar to the NH_3 emission mapped by Bachiller et al. (1987) and to the continuum emission mapped by Hatchell et al. (2005) at 850 μm and Enoch et al. (2006) at 1.1 mm. Such a good agreement between maps suggests that these tracers reflect the true distribution of dense gas in the region. The $C^{18}O$(1–0) emission, on the other hand, shows little contrast over the map and and peaks at a different position. The brightest $C^{18}O$(1–0) is located between the A and B cores of IC348-SW1, and the IC348-SW2 group of N_2H^+ cores coincides with a region of relatively weak $C^{18}O$ emission. This contrast between the $C^{18}O$ maps and the maps of N_2H^+, NH_3, and the continuum is unlikely to result from optical depth effects, as the $C^{18}O$(1–0) lines are less than 4 K in intensity and therefore not optically thick (the thick CO(2–1) lines are typically 20 K bright). It most likely results from $C^{18}O$ being strongly depleted at the highest densities. $C^{18}O$ (and CO) depletion due to freeze out onto dust grains is a common phenomenon in the cold, low-turbulence cores of clouds like Taurus, were it is by now well characterized (e.g., Caselli et al. 1999; Tafalla et al. 2002). Its finding in the warmer and more turbulent cores of IC348-SW indicates that CO depletion occurs at a relatively broad range of conditions.

To estimate the mass of each dense core we use the N_2H^+ emission. We first estimate the central H_2 column density $N(H_2)$ by assuming an N_2H^+ excitation similar to the one found in Taurus, and an N_2H^+ abundance of 1.5×10^{-10} (also as found in Taurus, e.g., Tafalla et al. 2004). This method produces H_2 column densities for cores A, B, and C that agree within a factor of 2 with the continuum-based estimates by Enoch et al. (2006), and we take this factor as indication of the level of un-

[1] FCRAO is supported in part by the National Science Foundation under grant AST 94-20159, and is operated with permission of the Metropolitan District Commission, Commonwealth of Massachusetts.

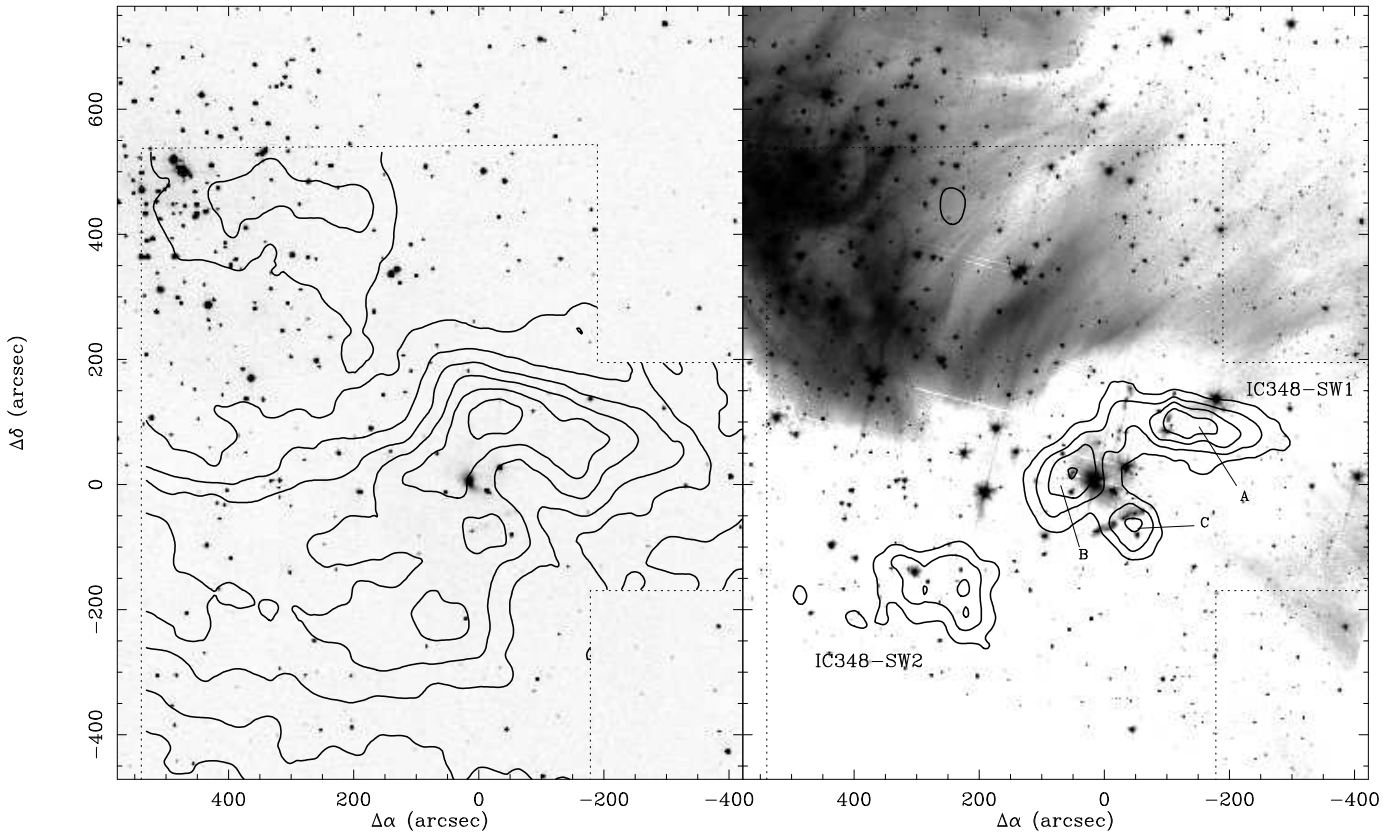

Fig. 1. FCRAO maps of the molecular gas in the south-western part of the IC 348 cluster. *Left:* $C^{18}O(1–0)$ integrated intensity map in contours superposed on the K-band 2MASS image. The $C^{18}O$ emission forms an arc that partly surrounds the IC 348 cluster (located at the top left). Right: $N_2H^+(1–0)$ emission (contours) superposed on the Spitzer IRAC1 (3.6 μm) image. The dense gas traced by N_2H^+ forms two groups of dense cores, IC348-SW1 and IC348-SW2, and a small condensation toward the cluster center. The map center is at α_{2000}=03:43:58.8, δ_{2000}=32:01:51, and the first contour and interval is 0.5 K km s^{-1} for $C^{18}O(1–0)$ and 1 K km s^{-1} for $N_2H^+(1–0)$. The dashed line indicates the region covered by the FCRAO observations. The $C^{18}O(1–0)$ map has been convolved to a final resolution of 65″ (FWHM) to filter out high frequency noise.

certainty of our estimate. We then measure the core radius R from the N_2H^+ map and assume an internal density structure of a critical Bonnor-Ebert sphere (e.g., Alves et al. 2001). In this way, the mass of the core is given by

$$M = 1.6 \left(\frac{N(\mathrm{H_2})}{10^{22}\ \mathrm{cm^{-2}}}\right)\left(\frac{R}{0.1\ \mathrm{pc}}\right)^2 M_\odot.$$

With this approximation, we derive masses of 9, 7, and 3 $M_\odot$ for cores A, B, and C, respectively, which are in reasonable agreement with the NH_3-based mass estimates of Bachiller et al. (1987). For the IC348-SW2 group of cores, we derive masses of 5 $M_\odot$ (western core) and 1.5 $M_\odot$ (eastern core), and for the core close to the center of the IC 348 cluster, we estimate an approximate mass of 1 $M_\odot$.

We have explored the velocity structure of IC348-SW1 and SW2 using the $N_2H^+(1–0)$ data, and we illustrate the main features with the two position-velocity (PV) diagrams of Fig. 2. The PV diagram for SW1 follows a curved path along the horseshoe, and the diagram for SW2 follows the long axis of the region (PA = 60°). As the top panel shows, the A core presents a single velocity component with a small velocity gradient ($\approx$ 1.3 km s^{-1} pc^{-1}) and a peak at around 8.6 km s^{-1}. The B and C cores, on the other hand, present lines with two peaks separated by about 0.5 km s^{-1}, being brighter the blue component in core B and the red component in core C. The presence of these two components seems not to result from an overlap between the cores, as each core appears distinct and centrally concentrated in the map of Fig. 1. In addition, the weaker red component of core B peaks at the same position as the brighter blue component, as if the two were correlated, and a similar but weaker correlation can be seen in core C. This behavior suggests that in each core the two components have a common origin. As we will see in the next section, the B and C cores are affected by outflows that have already accelerated part of the ambient gas (as seen in CO). It is therefore likely that the N_2H^+ components arise from outflow acceleration, as it has been previously found in other systems like L1228 (Tafalla & Myers 1997).

The velocity structure of SW2, on the other hand, is simpler than that of SW1. The $N_2H^+(1–0)$ line presents a single peak over the region, and there is a velocity gradient again at the level of 1.3 km s^{-1} pc^{-1}. This velocity gradient could represent a smooth change in the central velocity over SW2 or result from the two cores of SW2 having different velocities at the level of

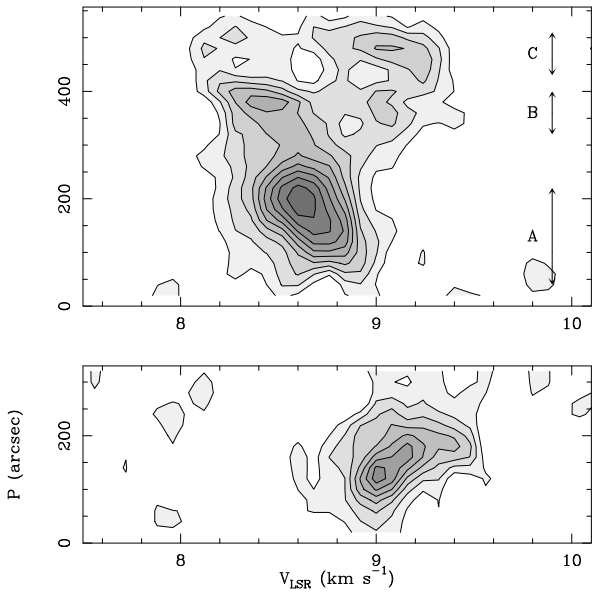

Fig. 2. Position-velocity diagrams of the N_2H^+(JF_1F=101-012) ("isolated component") emission toward IC348-SW1 (top) and IC348-SW2 (bottom). For IC348-SW1, the position axis follows a curved path that intersects the peaks of the A, B, and C cores, and the the approximate location of each core is indicated with arrows to the right. For IC348-SW2, the position axis follows a straight line with PA = 60°. In both panels, the first contour and interval are 0.1 K.

0.2 km s^{-1}. The contrast with the double-component velocity structure of SW1 may result from the SW2 region having no evidence for star formation and or outflows (see below).

4. Molecular outflows

We have searched for molecular outflows the IC348-SW1 and IC348-SW2 regions using CO(1–0) and CO(2–1) observations. No outflows were found towards IC348-SW2, while at least three outflows (two newly detected in CO) were found in IC348-SW1. To simplify the presentation, we separate the outflow velocity regime into "fast" and "slow."

4.1. Fast gas

We define as "fast" the gas that moves at more than 5 km s^{-1} with respect to the ambient cloud (ambient V_{LSR} = 8.6 km s^{-1} in IC348-SW1). This 5 km s^{-1} value corresponds to ten times the typical FWHM of the N_2H^+ line in IC348-SW1, and therefore guarantees the absence of contamination by ambient emission. The exact choice of the value, however, has little effect on the following discussion.

As Fig. 3 shows, the fast regime is dominated by two bipolar outflows, each centered on a bright 1.2mm compact source. The southern outflow is the well-known HH211 system, first identified by McCaughrean et al. (1994) from its H_2 emission, and later mapped at high resolution in CO and SiO by Gueth & Guilloteau (1999), Chandler & Richer (2001), Palau et al. (2006), and Hirano et al. (2006). The mm

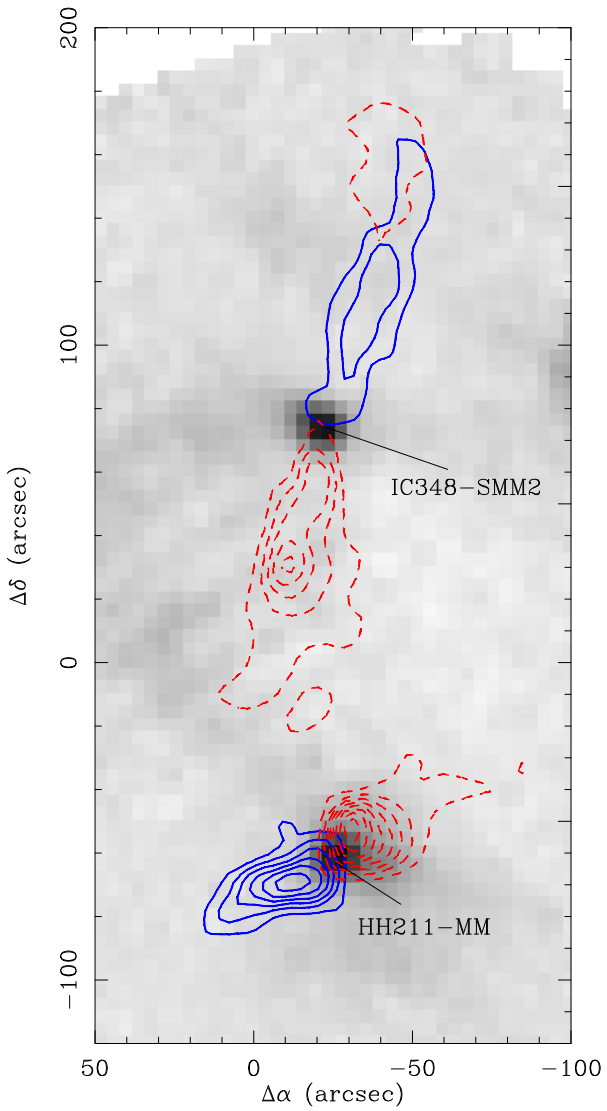

Fig. 3. Fast outflows in IC348-SW1. The contours show the CO(2–1) emission between 5 and 25 km s^{-1} with respect to ambient cloud (at V_{LSR} = 8.6 km s^{-1}). The solid blue contours represent blueshifted gas and the dashed red contours represent redshifted gas. The grey scale shows the 1.2 mm continuum emission. The two bright mm sources at the intersections of the red and blue contours are IC348-SMM2 (top) and HH211-MM (bottom). Offsets as in Fig. 1, and first contour and contour interval is 3 K km s^{-1}.

peak at its center have been variously referred as HH211-mm by (McCaughrean et al. 1994) or SMM1 (Walawender et al. 2006). The second fast outflow coincides with the extended H_2 emission detected by McCaughrean et al. (1994) (their H_2 "chain") and Eislöffel et al. (2003) (their "region 1"), and it also coincides with the HH797 A and B features recently observed in [S II] by Walawender et al. (2005). Compared with the optical and IR data, our CO observations provide velocity information, and show that the outflow is bipolar with respect to the northern mm source (referred as IC348 MMS by Eislöffel et al. 2003 and as SMM2 by Walawender et al. 2006). The CO data, therefore, shows un-

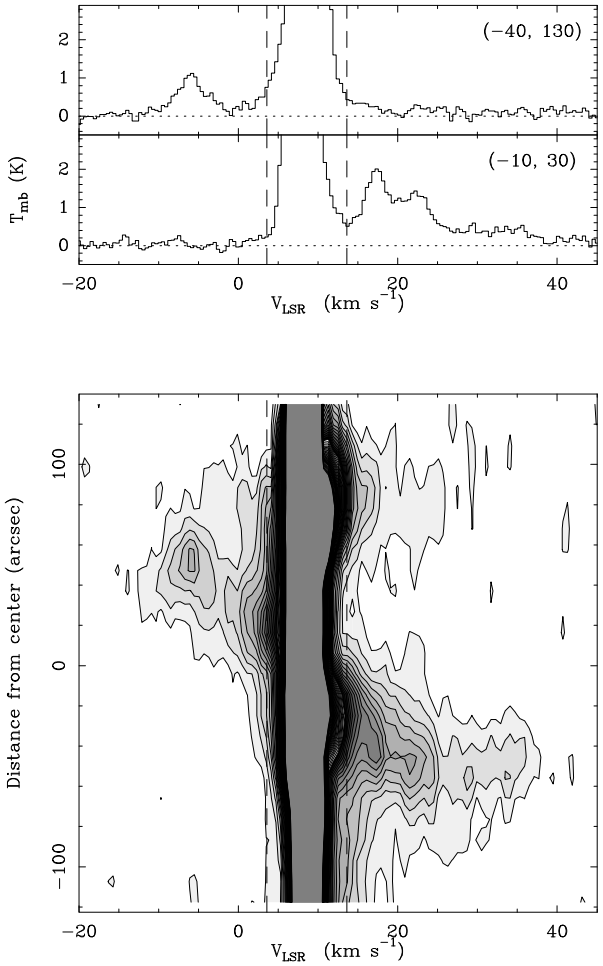

Fig. 4. CO(2–1) spectra and position velocity (PV) diagram along the IC348-SMM2 outflow. The spectra present secondary peaks of high velocity emission ("bullets") at positions symmetrically located with respect to SMM2. The PV diagram shows how the outflow speed increases with distance from SMM2 and how the bullets are highly localized in both velocity and position. Note that the offset in the spectra are referred to the map center (Fig. 1), so SMM2 is at (−25″, 75″), while in the PV diagram, the position axis measures distance from SMM2. The dashed lines mark the boundary of fast regime. First contour an interval in the PV diagram are 0.1 K.

ambiguously that SMM2 powers the outflow (we will follow the Walawender et al. 2006 notation in the following discussion).

The HH211 and SMM2 outflows present several differences and similarities. HH211 is more compact than the SMM2 outflow, and although this may indicate an intrinsic difference between the outflows it could also result from a projection effect. Indeed, the SMM2 outflow presents some mixing of blue and red emission at low velocities (see below), which suggests that the flow runs close to the plane of the sky. In any case, both outflows seem to belong to the class of highly collimated flows. The interferometric data of Gueth & Guilloteau (1999) (also Chandler & Richer 2001; Palau et al. 2006; Hirano et al. 2006) show that the fastest part of the HH211 outflow is unresolved with arcsecond beams. The SMM2 outflow, on the other hand, is unresolved by our 11″ single-dish beam at the highest speeds. In addition, its CO spectra present at some positions secondary peaks of high velocity (see Fig. 4). These peaks, often called "bullets," are commonly associated with jet-like components in outflows (Bachiller et al. 1990), and their presence in the SMM2 system suggest the existence of extremely collimated gas. Interferometric observations of the SMM2 outflow are necessary to further characterize this component.

4.2. Slow gas

The threshold of 5 km s^{-1} used for the fast gas guarantees the absence of contamination by low-velocity material, but limits our sensitivity to weak or slow outflows. As a second step in our outflow search, we now explore the gas moving at velocities lower than this threshold, but still avoiding contamination from ambient gas. We have experimented with different velocity ranges and have found that the gas moving between 3 and 5 km s^{-1} from the ambient cloud still seems free from ambient contamination. For this reason, we will refer to this range as the "slow gas" regime, although it should be noted that this gas still moves supersonically with respect to the ambient cloud.

Figure 5 shows the slow gas regime of CO(2–1) toward the IC348-SW1 region (solid blue and dashed red contours) superposed to the N_2H^+(1–0) emission (dotted lines) and the Spitzer Space Telescope 24 μm image from the Cores to Disks (c2d) Legacy Project (Evans et al. 2003). The HH211 and IC348-SMM2 outflows are still the dominant elements of the slow CO emission, but a number of new features are visible. In the IC348-SMM2 outflow, there is a red component at the end of the northern blue lobe and a blue arc to its northeast. The origin of these components is suggested by their location with respect to the dense gas traced by N_2H^+. The N_2H^+ emission shows that the SMM2 outflow runs between the A and B cores and that the two anomalous features occur at the edge of the region, where the outflow leaves the dense gas and encounters the surrounding medium. The anomalous red emission continues the direction of the flow and coincides with a region where the shocked H_2 emission becomes brighter and broader (McCaughrean et al. 1994; Eislöffel et al. 2003; Walawender et al. 2006). This suggests that the anomalous red CO emission results from a broadening of the outflow when it encounters the surrounding lower density medium, as it has been observed in other systems like the Orion HH212 outflow (Lee et al. 2000). The outflow broadening may result from a change in the gas regime from isothermal to adiabatic, and if the outflow moves close to the plane of the sky, it can naturally produce the observed superposition of blue and red gas (e.g., Cabrit et al. 1988). The blue arc to the east, on the other hand, has a less clear origin. It could result from a strong deflection of the outflow, but there is no evidence for an obstacle along the outflow path. In fact, the wind responsible for the outflow seems to continue unimpeded past the region with anomalous blue emission. This is inferred from the long and highly collimated chain of H_2 emission, which continues at least up to the

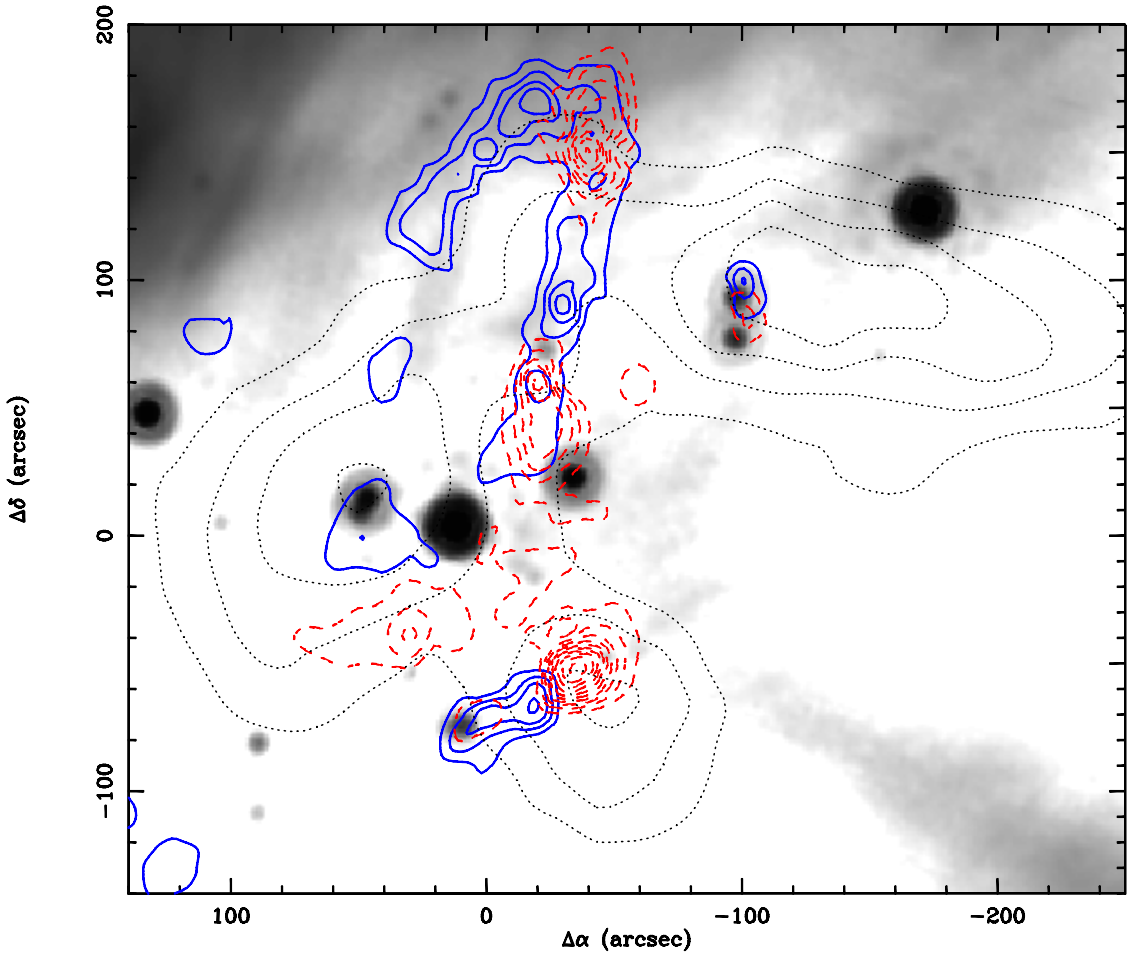

Fig. 5. Slow outflow gas toward IC348-SW1. The contours show the CO(2–1) emission integrated between 3 and 5 km s^{-1} with respect to the ambient cloud (at $V_{\rm LSR}$ = 8.6 km s^{-1}). The solid blue lines represent blueshifted emission, and the dashed red lines represent redshifted emission. The black dotted contours indicate the N_2H^+(1–0) emission also shown in Fig. 1, and the grey-scale image in the background is the 24 μm Spitzer MIPS image from the c2d Legacy Project. At least three CO bipolar outflows are present in the region (see text). Offsets as in Fig. 1, and first CO contour and contour interval is 1 K km s^{-1}.

bright "1-w" knot of Eislöffel et al. (2003). Such a knot is located at offset (−54″, 243″) with respect to our map center, and therefore is well aligned with the collimated CO outflow past the region of anomalous blue gas (it is in fact so much further north from the blue gas that it lies outside our map). A more likely interpretation, therefore, is that the blue gas is not related to the outflow. Fig. 5 shows that the blue gas forms an arc parallel to the dense gas distribution traced by N_2H^+ and that approximately points towards the center of the IC 348 cluster (about 1 pc away in projection). We have seen from the $C^{18}O$ emission (Fig. 1) that the cluster seems to have excavated a circular hole in the molecular gas, so it is possible that the blue CO emission results from this destructive action of the cluster and not from the CO flow. This would also explain naturally the shift to the blue, as the IC348-SW1 region is located slightly in front of the cluster (Section 3), so the dense gas will be pushed from behind.

After the CO emission associated directly with the HH211 and SMM2 outflows, the next brightest peak of the slow regime occurs near (30″, −40″) and is part of a region of red gas that lies along the southwestern edge of core B (Fig. 5). This red gas is not continuously connected to the red lobe of SMM2, but the presence of another region of red emission near (−20″, −20″) and a number of nearby H_2 knots in the images of Walawender et al. (2006) suggests that the two pieces of red gas are indeed connected and associated with the southern lobe of the SMM2 outflow. If so, the southern lobe would be approximately as long as the northern lobe.

About 40″ north of the bright red peak just discussed, there is a triangular patch of blue gas whose northern vertex coincides with the "region 3" of H_2 emission in the study of Eislöffel et al. (2003). As Fig. 5 shows, this region also presents bright 24 μm emission, which suggests the presence of an additional embedded object.

A better defined feature of the slow CO emission occurs near (−100″, 100″). There, a blue and a red lobe of gas form a very compact outflow at the eastern edge of core A. This newly found CO flow runs approximately north-south, parallel to the SMM2 outflow, and seems associated with the "region 2" of H_2 emission identified by Eislöffel et al. (2003). The close-up view in Fig. 6 shows that the outflow has diffuse H_2 emission both towards its north and south lobes, and

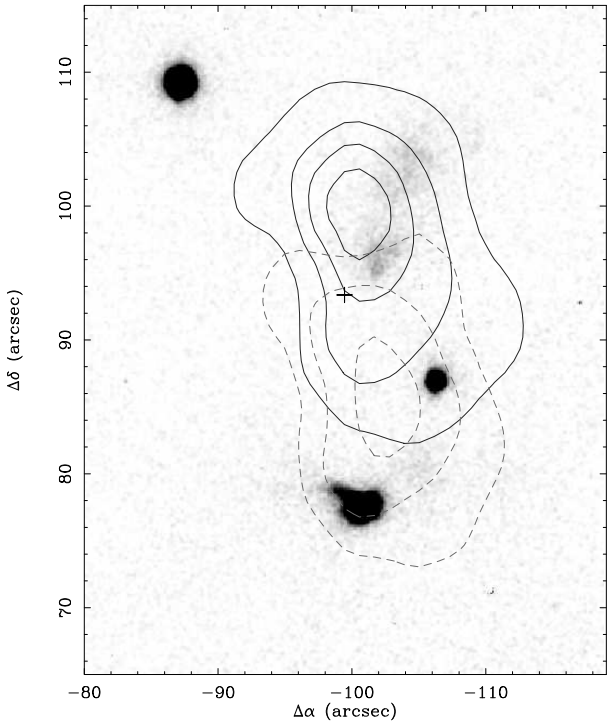

Fig. 6. IC348-SMM3 outflow. The solid (blue) and dashed (red) contours indicate the CO(2–1) emission blueshifted and redshifted between 3 and 5 km s^{-1} with respect to the ambient cloud (slow outflow regime). The grey scale shows our UKIRT K-band image and the plus sign indicates the position of a 24 μm source. Offsets as in Fig. 1, and first contour and interval is 1.0 K km s^{-1}.

that its center lies about 8″ to the northeast of 2MASS source 03435056+3203180. The 2MASS source, however, is probably not the outflow source, as its JHK colors are consistent with those of a background or TTauri star (Lada & Adams 1992). A more likely candidate for the exciting source is provided by the 24μm Spitzer image. As Fig. 5 shows, there are two sources superposed to the CO emission, one toward the geometric center of the outflow (plus sign in Fig. 6) and the other coinciding with the bright H_2 knot at the end of the red lobe. Both 24 μm sources are different from the 2MASS source and are classified as YSO candidates in the current c2d catalog (Evans et al. 2005). The northern source, close to the outflow center, is most likely the driving source of the outflow, while the second source may result not from an embedded object but from line emission in the shock. A similar situation seems to occur toward the HH211 outflow, where the end of the blue lobe coincides with a bright 24 μm peak (Fig. 5). This 24 μm peak is also classified as a YSO candidate in the c2d catalogue, but it has no evidence for mm or submm emission (e.g., Fig. 3), while its position coincides with the point of strongest IR and optical shock emission in HH211 (e.g., Walawender et al. 2006). Line emission from outflow shocks near 24 μm is in fact expected from theoretical grounds. Hollenbach & McKee (1989) predict that the [S I] line at 25.2 μm and the [Fe II] line at 26.0 μm will be among the brightest atomic fine-structure lines in shocks at densities between 10^4 and 10^6 cm^{-3}, typical of dense cores (their Fig. 7), and these two lines fall inside the 4.7 μm-wide bandpass of the 24 μm MIPS detector. Bright [S I] emission at 25.2 μm has in fact been observed by Noriega-Crespo et al. (2004) toward the Cepheus E outflow, which is also powered by a very young object, so this emission is also expected from the outflows in the IC348-SW1 region. Until spectroscopic observations of the 24 μm sources are available, their association with a YSO remains uncertain (the lower wavelength Spitzer bands of IRAC can also be contaminated by H_2 emission, Jørgensen et al. 2006). A more secure counterpart for the exciting source of the compact outflow is provided by the submm continuum emission observed by different authors. Source 15 of Hatchell et al. (2005), source 102 of Enoch et al. (2006), and source SMM3 of Walawender et al. (2006) all coincide with the approximate center of the CO outflow, and even our 1.2 mm observations, where the source is close to the map edge, show evidence of emission at the 100 mJy level. Given this more secure identification of the source at submm wavelengths, from now on we will refer to the outflow driving source as IC348-SMM3.

Table 1. Outflow energetics

Outflow	Mass ($M_\odot$)	Momentum ($M_\odot$ km s^{-1})	Energy (erg)
HH211-MM	$1.5\ 10^{-2}$	$1.5\ 10^{-1}$	$6\ 10^{43}$
IC348-SMM2	$3.3\ 10^{-2}$	$3.1\ 10^{-1}$	$1\ 10^{44}$
IC348-SMM3	10^{-3}	$4\ 10^{-3}$	$4\ 10^{41}$

4.3. Outflow energetics and nature of the powering sources

We calculate the mass, momentum, and energy of the outflows using the CO(2–1) emission, which we assume is optically thin in the outflow regime and that has an excitation temperature of 20 K, as suggested by the ambient peak intensities (these two assumptions make our estimate a lower limit). We also assume a CO abundance of $8.5\ 10^{-5}$ (Frerking et al. 1982) and make no correction for outflow inclination. Neglecting the contribution of gas moving at less than 3 km s^{-1} from the ambient cloud (V_{LSR} = 8.6 km s^{-1}), we obtain the outflow parameters listed in Table 1. Although the HH211 outflow has been studied before, previous estimates of its parameters were based on interferometer data, and therefore missed a significant fraction of the emission. The Table 1 values, therefore, contain the first full estimate of the HH211 energetics.

As can be seen in the table, the HH211 and SMM2 outflows have very similar parameters. Their mass, momentum, and energy differ by a factor of 2 or less, which is little given all the uncertainties involved. The slightly larger values of the SMM2 flow (despite its location closer to the plane of the sky) may arise from the larger luminosity of the source: 8 $L_\odot$ versus the 4 $L_\odot$ of HH211-MM (Froebrich et al. 2003; Eislöffel et al. 2003). These similar energetics, together with the similar speeds and high collimation, suggest that the powering sources of the HH211 and SMM2 outflows share simi-

lar physical properties and evolutionary state. Froebrich et al. (2003) and Eislöffel et al. (2003) have classified these sources as Class 0 (André et al. 1993), and the outflow parameters in Table 1 confirm that the two objects belong to the youngest protostellar phase.

The IC348-SMM3 outflow, on the other hand, has a very small energy content, close to the detection limit of our survey. Compared with the HH211 and SMM2 outflows, the SMM3 outflow is about one order of magnitude less massive and has two orders of magnitude less kinetic energy. These numbers, together with the small spatial extent of the CO emission (about 30″ or 0.04 pc) suggest that the flow is powered by a source of much lower luminosity than HH211-MM or SMM2. The exact luminosity of SMM3, unfortunately, is not well constrained. The 24 μm flux may be contaminated by outflow emission (see above), and no data close to the peak of the SED are available yet (the IRAS data are confused by the extended emission from the IC 348 cluster). Although the outflow parameters suggest that SMM3 is a low luminosity source, it is unlikely that its energy output is as low as that of the very low luminosity object (VELLO) L1014-IRS (0.09 $L_\odot$, Young et al. 2004). For this object, Bourke et al. (2005) estimate an outflow mass about 70 times smaller and a kinetic energy at least two orders of magnitude lower than those of the SMM3 outflow. Although the interferometric data used to derive the L1014-IRS outflow parameters only provide a lower limit because of filtering of the extended emission, the difference in values is too large to be explained as an artifact. It seems therefore likely that SMM3 is more luminous than 0.09 $L_\odot$.

5. Star formation in IC348-SW and its relation to the IC 348 cluster

We have seen that the IC348-SW1 group of cores is relatively rich in young stellar objects. Sources HH211-MM, IC348-SMM2, and IC348-SMM3 all drive bipolar outflows and are therefore YSOs likely formed in IC348-SW1 within the last $\approx 10^5$ yr (Class 0 objects are even younger, André et al. 1993). The IC348-IRS1 object, whose discovery provided the first indication that star formation was still ongoing in IC 348 (Strom et al. 1974), has a less clear status. It has been interpreted as a late B star with an edge-on disk by Boulard et al. (1995), but recent IR observations by Luhman et al. (1998) suggest that it has an early M spectral type. Its large extinction (Luhman et al. 1998) and reflection nebulosity Boulard et al. (1995) indicate youth, but the lack of a well defined outflow (Section 4.2) suggests that it is more evolved than the other three sources; a complete spectral energy distribution is still needed to properly classify this YSO. Other young objects in the region have been identified in the surveys of Herbig (1998) and Luhman et al. (1998), who searched for evidence of H_α emission and IR excess. Among these objects, IfAHA 7 and 8 stand out for lying projected onto the N_2H^+ emission and having H_α equivalent widths of classical T Tauri stars (35 and 30 Å for IfAHA 7 and 8, respectively, Herbig 1998). Given their expected age ($\approx 10^6$ yr, Luhman et al. 1998), however, it is unclear whether these stars have originated from the IC348-SW1 group of cores or they belong to a more distributed stellar population that has already drifted from its natal place. Even discounting these older objects, the presence of 4 YSOs, two of them of Class 0, makes IC348-SW1 the most active star-forming site of the IC 348 cluster.

The study of IC348-SW1 may help elucidate the process of star formation in the IC 348 cluster. Lada & Lada (1995) have found that the stellar distribution in the outer cluster presents significant substructure. In addition to a central core of stars with a radius of 0.5 pc, the authors identify eight subclusters, each containing 5-20 sources within a radius of 0.1-0.2 pc. The sizes of these subclusters match the approximate size of the IC348-SW1 and SW2 regions as measured from the N_2H^+ maps (radii 0.1-0.3 pc), and this suggests a connection between the two types of objects. Using the 4 YSOs identified in IC348-SW1, which lie inside a circle of 85″ radius, we crudely estimate a stellar density of 70 stars pc^{-2}. This density is already half the mean stellar density of the Lada & Lada subclusters, and equals the density of their subcluster "c." Adding the nearby sources IfAHA 7 and 8 (Herbig 1998) and sources 49, 160, and 124 from the Luhman (1999) catalog further enriches the stellar census toward IC348-SW1, to which new sources will be incorporated if the cores form additional stars with the dense gas still available. The final result of star formation in IC348-SW1 and its vicinity will therefore be a stellar density enhancement similar to the subclusters found by Lada & Lada (1995).

To explore whether star formation in regions like IC348-SW1 is a viable mechanism to produce the observed subclustering, we need to investigate whether the number of stars found in subclusters is consistent with their production rate and dispersal time scale. A given group of stars will appear as a distinct density enhancement until its members drift apart due to proper motions, and for the case of IC348-SW1 we can estimate this timescale from the typical velocity difference between its constituent cores (the linewidths may be contaminated by core disruption, see section 3). From our N_2H^+(1–0) spectra, we estimate that the typical core-to-core velocity difference is less than 0.3 km s^{-1}, in agreement with the NH_3 estimate of Bachiller et al. (1987). This line-of-sight estimate implies a plane of the sky dispersion close to 0.4 km s^{-1} if the velocity field is isotropic. As the subclusters have a typical radius of 0.15 pc Lada & Lada (1995), stars will travel a diameter distance in about 0.75 Myr, which we take as a typical stellar group lifetime. To calculate the number of stars formed in this time, we assume that the cluster has been forming stars at a constant rate over the last 3 Myr (Muench et al. 2003), and that half of its 380 stars have formed in the outer cluster (Lada & Lada 1995). Thus, over the last 0.75 Myr, about 47 stars have formed in the outer IC 348 cluster. This number should be compared with the 82 stars found by Lada & Lada (1995) in the subclusters of the halo, but first we need to subtract the contamination by the more diffuse cluster population. Dividing the number of non subcluster objects in the outer cluster by the area of this region, we estimate that the contamination fraction is 1/3 (density of diffuse population is 50 stars pc^{-2} and mean density in a subcluster is 150 stars pc^{-2}). This implies that there are about 55 stars in the subclusters of the outer IC 348, which is roughly consistent with the 47 stars expected if

the stars formed in regions like IC348-SW1. The subclustering structure, therefore, could have resulted from star formation in aggregates of dense cores like the ones we have studied. Indeed, if star formation in these loose aggregates produces a different proportion of low mass stars than the formation in a more compact environment, likely responsible for the central stellar core of IC 348, the difference may help explain the radial dependence of the IMF found by Muench et al. (2003).

Finally, we note that the velocity dispersion between aggregates of cores seems to be larger than the velocity dispersion between the cores of a given aggregate. Our N_2H^+ mapping of the IC 348 vicinity is not complete enough to determine the full statistics of the aggregate-to-aggregate kinematics, but it already provides some interesting hints. The SW1, SW2 aggregates and the core towards the IC 348 center have mean LSR velocities of 8.6, 9.1, and 7.9 km s^{-1}, respectively, from which we estimate a (necessarily crude) rms value of 0.6 km s^{-1} together with a trend for the velocity difference to increase with distance between aggregates. This dispersion is larger than the difference of about 0.3 km s^{-1} found between the cores of IC348-SW1, and suggests that most of the initial velocity dispersion between the stars in the core will result from the relative velocities of the aggregates and not from the small scale turbulence inside the aggregates. It also suggests that the stars formed from a given aggregate may keep a distinct velocity pattern for about 0.75 Myr, which should be testable with a proper motion study of the subclusters.

6. Summary

We have mapped the molecular gas south-west of the IC 348 young cluster in $C^{18}O$(1–0), N_2H^+(1–0), and CO(2–1). Combining these data with observations of the young stars and YSOs in the NIR and mm continuum, we have reached the following conclusions.

1. The dense gas south-west of IC 348 is concentrated in two regions, referred here as IC348-SW1 and IC348-SW2, each containing several cores of a few solar masses of material. The two regions are embedded is lower density gas and they seem located in the front part of the IC 348 cluster. While IC348-SW1 is actively forming stars, IC348-SW2 seems quiescent.

2. The distribution of N_2H^+(1–0) emission is similar to the distribution of NH_3 and submm continuum mapped by previous authors, but differs significantly from that of $C^{18}O$(1–0). As the rare isotope is not optically thick, the disagreement suggests that the CO molecule is depleted at the core centers (likely due to freeze out onto grains) as previously seen in the more quiescent cores of Taurus.

3. The fast CO emission ($|\Delta V| > 5$ km s^{-1} with respect to the ambient cloud) is dominated by two highly collimated outflows, each associated with a bright mm/submm source. The first outflow is the molecular counterpart of HH211 and has already been mapped using interferometers by a number of authors. The second outflow, not previously mapped in CO, is associated with a previously known chain of H_2 emission and several HH objects, and is referred here as the IC348-SMM2 outflow. The characteristics and energetic content of the two outflows are consistent with them being excited by Class 0 sources.

4. At low velocities ($3 < |\Delta V| < 5$ km s^{-1}), the CO emission presents additional features associated with the SMM2 outflow and (probably) the interaction of the cluster and the dense gas. In addition, we find a compact outflow associated with with a mm/submm object (SMM3) also detected at 24 μm. The small size and low energy content of this new outflow suggests that it is powered by a source of rather low luminosity.

5. The ongoing star formation activity in IC348-SW1 is producing a significant stellar density enhancement, similar to others previously identified in the halo of the IC 348 cluster from NIR observations. From an estimate of the production rate and dispersal timescale of aggregates like IC348-SW1, we conclude that similar episodes of star formation could have originated the substructure seen in the IC 348 cluster.

Acknowledgements. We thank Chris Davis for obtaining the infrared data of SMM3 through a service program at UKIRT, Jennifer Hatchell for providing us with her 850μm data of the region, and Jorge Grave for creating a color version of Fig. 1. MT and RB acknowledge partial support from grant AYA2003-7584. This research has made use of NASA's Astrophysics Data System Bibliographic Services, the SIMBAD database, operated at CDS, Strasbourg, France, and the Two Micron All Sky Survey, which is a joint project of the University of Massachusetts and the Infrared Processing and Analysis Center/California Institute of Technology, funded by the National Aeronautics and Space Administration and the National Science Foundation. The DSS was produced at the Space Telescope Science Institute under US Government grant NAG W-2166. This work is based in part on observations made with the Spitzer Space Telescope, which is operated by the Jet Propulsion Laboratory, California Institute of Technology under a contract with NASA.

References

Alves, J., Lada, C.J., Lada, E.A. 2001, Nat, 409, 159
André, P., Ward-Thompson, D. & Barsony, M. 1993, ApJ, 406, 122
Bachiller, R., & Cernicharo, J. 1986, A&A, 166, 283
Bachiller, R., Cernicharo, J., Martín-Pintado, J., Tafalla, M., & Lazareff, B. 1990, A&A, 231, 174
Bachiller, R., Guilloteau, S. & Kahane, C. 1987, A&A, 173, 324
Boulard, M.-H., Caux, E., Monin, J.-L., Nadeau, D., & Rowlands, N. 1995, A&A, 300, 276
Bourke, T.L., Crapsi, A., Myers, P.C., et al. 2005, ApJ, 633, L129
Cabrit, S., Goldsmith, P.F., Snell, R.L. 1988, ApJ, 334, 196
Caselli, P., Walmsley, C.M., Tafalla, M., Dore, L., Myers, P.C. 1999, ApJ, 523, L165
Chandler, C.J. & Richer, J.S. 2001, ApJ, 555, 139
Eislöffel, J., Froebrich, D., Stanke, T. & McCaughrean, M. J. 2003, ApJ, 595, 259
Enoch, M.L., Young, K.E., Glenn, J., et al. 2005, ApJ, 638, 293
Evans, N.J., II, Allen, L.E., Blake, G.A., et al. 2003, PASP, 115, 965
Evans, N.J., II, Harvey, P.M., Dunham, M.M., et al. 2005, "Third Delivery of Data from the c2d Legacy Project: IRAC and MIPS," (Pasadena, SSC)

Frerking, M.A., Langer, W.D., & Wilson, R.W. 1982, ApJ, 262, 590
Froebrich, D., Smith, M. D., Hodapp, K.-W. & Eislöffel, J. 2003, MNRAS, 346, 163
Gueth, F. & Guilloteau, S. 1999, A&A, 343, 750
Hatchell, J., Richer, J.S., Fuller, G.A., et al. 2005, A&A, 440, 151
Herbig, G.H. 1998, ApJ, 497, 736
Hirano, N., Liu, S.-Y., Shang, H., et al. 2006, ApJ, 636, L141
Hollenbach, D., & McKee, C.F. 1989, ApJ, 342, 306
Jørgensen, J.K., Harvey, P.M., Evans, N.J., II, et al. 2006, ApJ, in press [astro-ph/0603547]
Lada, C.J. & Adams, F.C. 1992, ApJ, 393, 278
Lada, E.A. & Lada, C.J. 1995, AJ, 109, 1682
Lee, C.-F., Mundy, L.G., Reipurth, B., Ostriker, E.C., & Stone, J.M. 2000, 542, 925
Luhman, K.L., Rieke, G.H., Lada, C.J., & Lada, E.A. 1998, ApJ, 508, 347
Luhman, K. L. 1999, ApJ, 525, 466
Kirk, H., Johnstone, D., & Di Francesco, J. 2006, ApJ, in press [astro-ph/0602089]
McCaughrean, M. J., Rayner, J. T. & Zinnecker, H. 1994, ApJ, 436, L189
Muench, A.A., Lada, E.A., Lada, C.J., et al. 2003, AJ, 125, 2029
Najita, J.R., Tiede, G.P., & Carr, J.S. 2000, ApJ, 541, 977
Noriega-Crespo, A., Moro-Martín, A., Carey, S., et al. 2004, ApJ, 154, 402
Palau, A., Ho, P.T.P., Zhang, Q., et al. 2006, ApJ, 636, L137
Preibisch, T. & Zinnecker, H. 2004, A&A, 422, 1001
Ridge, N.A., Di Francesco, J., Kirk, H., et al. 2006, AJ, 131, 2921
Strom, S. E., Strom, K. M., & Carrasco, L. 1974, PASP, 86, 798
Sun, K., Kramer, C., Ossenkopf, V., et al. 2006, A&A, 451, 539
Tafalla, M., & Myers, P.C. 1997, ApJ, 491, 653
Tafalla, M., Myers, P.C. Caselli, P., Walmsley, C.M., & Comito, C. 2002, ApJ, 569, 815
Tafalla, M., Myers, P.C. Caselli, P., & Walmsley, C.M. 2004, A&A, 416, 191
Young, C.H., Jørgensen, J.K., Shirley, Y.L., et al. 2004, ApJS, 154, 396
Walawender, J., Bally, J., & Reipurth, B. 2005, AJ, 129, 2308
Walawender, J., Bally, J., Kirk, H., et al. 2006, AJ, in press